

Nanoscale chemical mapping of laser-solubilized silk

Meguya Ryu¹, Hanae Kobayashi², Armandas Balčytis^{3,4},
Xuwen Wang³, Jitraporn Vongsvivut⁵, Jingliang Li⁶,
Norio Urayama², Vygantas Mizeikis⁷, Mark Tobin⁵,
Saulius Juodkazis^{3,8}, Junko Morikawa¹

¹Tokyo Institute of Technology, Meguro-ku, Tokyo 152-8550, Japan

²Nihon Thermal Consulting Co., 1-5-11, Nishi-Sinjuku, Shinjuku-ku, Tokyo 160-0023, Japan

³Nanotechnology facility, Swinburne University of Technology, John st., Hawthorn, 3122 VIC, Australia

⁴Center for Physical Sciences and Technology, Savanoriu ave. 231, LT-02300 Vilnius, Lithuania

⁵Infrared Microspectroscopy Beamline, Australian Synchrotron, Clayton, VIC 3168, Australia

⁶Institute for Frontier Materials, Deakin University, Geelong, VIC 3220 Australia

⁷Research Institute of Electronics, Shizuoka University, Naka Ku, 3-5-3-1 Johoku, Hamamatsu, Shizuoka 4328561, Japan

⁸Melbourne Center for Nanofabrication, Australian National Fabrication Facility, Clayton 3168, Melbourne, Australia

E-mail: sjuodkazis@swin.edu.au; morikawa.j.aa@m.titech.ac.jp

25August 2017

Abstract. A water soluble amorphous form of silk was made by ultra-short laser pulse irradiation and detected by nanoscale IR mapping. An optical absorption-induced nanoscale surface expansion was probed to yield the spectral response of silk at IR molecular fingerprinting wavelengths with a high ~ 20 nm spatial resolution defined by the tip of the probe. Silk microtomed sections of 1-5 μm in thickness were prepared for nanoscale spectroscopy and a laser was used to induce amorphisation. Comparison of silk absorbance measurements carried out by table-top and synchrotron Fourier transform IR spectroscopy proved that chemical imaging obtained at high spatial resolution and specificity (able to discriminate between amorphous and crystalline silk) is reliably achieved by nanoscale IR. A nanoscale material characterization using synchrotron IR radiation is discussed.

Keywords: silk, FT-IR, synchrotron radiation

1. Introduction

In analytical material science, absorption of IR light is used for fingerprinting (chemical imaging) of particular molecules, specific compounds, and provides insight into interactions in their immediate vicinity. However, challenges arise when this

information needs to be obtained from sub-wavelength and sub-cellular dimensions, in particular at IR and terahertz spectral bands of absorption [1] or scattering [2]. Optical properties of sub-wavelength structures and patterns have opened an entirely new direction in photonics and design of highly efficient optical elements for control of intensity, phase, polarisation, spin and orbital momenta of light based on flat planar geometries, yet rich in nanoscale features [3,4]. We aim at reaching that level of control in the domain of chemical spectral imaging. There, interpretation of data from near-field requires further knowledge of probe interaction with substrate, phase information of the reflected/transmitted light from sub-wavelength structures to reveal complex peculiarities of light-matter interactions at nanoscale and is now advancing with strongly concentrated efforts [5–10]. Recently, an electron tunneling control by a single-cycle terahertz pulse illuminated onto a tip of a scanning transmission microscope (STM) needle was demonstrated at 10 V/nm fields [11]. STM reaches an atomic precision in surface probing and its spectroscopic characterisation and can be carried out on a water surface [12].

Absorbance spectra quantify and identify the resonant molecules, chemical structures through their individual or collective excitations as detected in transmission (or inferred from reflection). By sweeping excitation wavelength through the fingerprinting region of a particular material, the usual optical excitation relaxation pathway ending with a thermal energy deposition into host material can be sensitively measured using an atomic force microscopy (AFM) approach [13,14] which opened up a rapidly growing AFM-IR field [15] (also known as nano-IR; Fig. 1(a)). How reliably one can determine IR properties with an AFM nano-tip based on the thermal expansion is currently still under debate due to a lack of knowledge of the actual anisotropy of thermal and mechanical properties at the nanoscale, 3D molecular conformation, alignment, and the interaction volume. To establish the correspondence between nano-IR and spectroscopy it is necessary to compare IR spectral imaging in near-field and far-field modes with nano-IR. Another challenge of the nano-IR technique is that a very thin sub-micrometer film has to be prepared and mounted on a thermally conductive substrate. Microtomed thin sections usually have thicknesses above the optimum and need to be embedded into an epoxy host which interferes with the nano-IR signal from micro-specimens.

In order to demonstrate that microtomed slices of samples with features at or below micrometers in lateral cross-section can be measured using nano-IR and provide reliable IR spectral information we acquired absorbance spectra from areas down to single pixel hyper-spectral resolution accessible on table-top FT-IR spectrometers, and at high-resolution which was achieved with a solid immersion lens using high-brightness synchrotron FT-IR microscopy. Such comparison of IR properties read out from nanoscale and far-field was carried out in this study using silk - a bio-polymer complex in its structure comprised of crystalline and amorphous building blocks [16–19].

Here, micrometer-thick slices of silk were used to measure thermal expansion under a specific wavelength of excitation with ~ 20 -nm-sharp AFM tips and to compare with

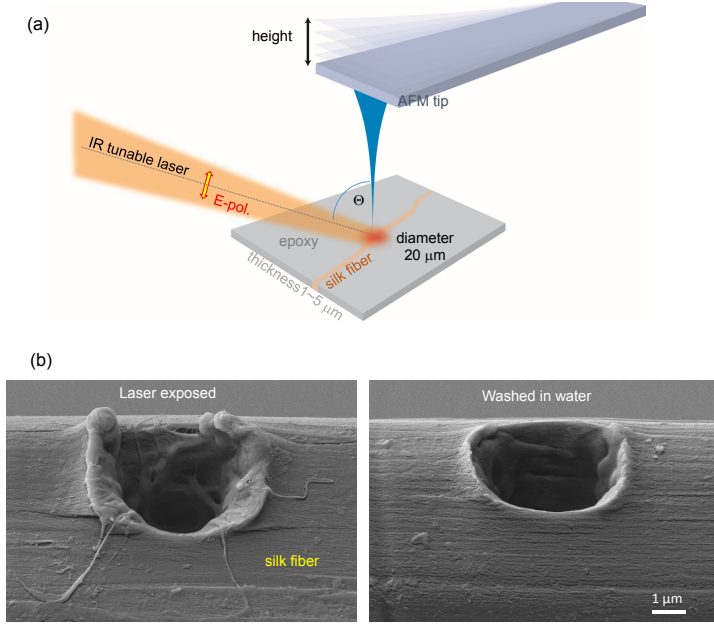


Figure 1. Principle of nano-IR: an AFM tip follows height changes induced by a spectral sweep of excitation at IR wavelengths ($\sim 6 \mu\text{m}$). IR laser beam is p-polarised and incident at $\Theta \simeq 60^\circ$ angle to minimise reflective losses (close to the Brewster angle) and to illuminate a much larger sample area while AFM readout occurs from a AFM needle contact ($\sim 20 \text{ nm}$) continuously scanned with 0.1 Hz frequency and digitised to obtain map with $x \times y = 25 \times 100 \text{ nm}^2$ pixels. AFM and nano-IR mapping was carried out at a selected excitation wavelength. (b) SEM images of silk fiber melted/amorphised by a single laser pulse as-fabricated and after immersion into water; laser wavelength 515 nm, pulse duration 230 fs, focused with objective lens with numerical aperture $NA = 0.5$, pulse energy 425 nJ, linear polarisation was along the fiber (different fibers exposed at the same conditions were used for the two images).

high-resolution spectra measured with ATR FT-IR method using synchrotron radiation at the Infrared Microspectroscopy (IRM) Beamline (Australian Synchrotron) as well as a table-top FT-IR spectrometer. Amorphisation of silk induced by single ultra-short laser pulses [19] has been spectroscopically recognised using nano-IR.

2. Samples and methods

Domestic (*Bombyx mori*) silk fibers, stripped of their sericin rich cladding [20], were probed during the spectroscopic imaging experiments. Pulsed laser radiation was used to induce local structural modifications of silk. The AFM-based nano-IR experiments with $\sim 25\text{-nm}$ -diameter tips were benchmarked against more conventional methods, such as attenuated total reflectance (ATR) at the Australian Synchrotron IRM Beamline ($\sim 1.9 \mu\text{m}$ resolution), and a table-top FT-IR spectrometer ($\sim 6 \mu\text{m}$ resolution).

For this set of experiments method-agnostic silk samples, in the form of thin slices, had to be prepared. For cross-sectional observation, the natural silk fibers were aligned and embedded into an epoxy adhesive (jER 828, Mitsubishi Chemical Co., Ltd.).

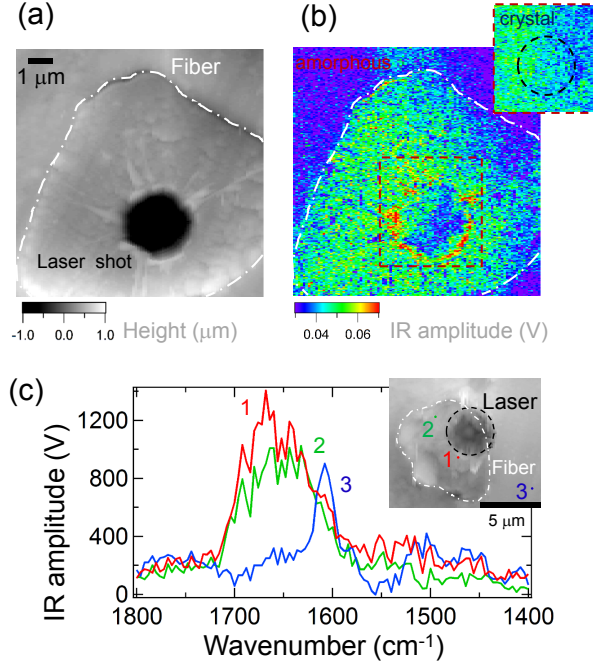


Figure 2. AFM (a) and chemical map at Amide I 1660 cm^{-1} band (b) measured with nano-IR; inset in (b) shows the ablation pit region imaged at crystalline band at 1700 cm^{-1} . (c) Point spectra measured on epoxy, amorphous-rich, and predominantly crystalline regions of the T-cross-section of a silk fiber; inset shows AFM image of a microtome slice of a silk fiber in the epoxy matrix and laser irradiated crater region.

Fibers fixed in the epoxy matrix were microtomed into $1\text{--}5\text{ }\mu\text{m}$ -thick slices which are mechanically robust enough to be measured using standard FT-IR setups without any supporting substrate. This was particularly important to increase sensitivity of the far-field absorbance measurements and to diminish reflective losses. Both longitudinal (L) and transverse (T) slices of the silk fibers were prepared by microtome (RV-240, Yamato Khoki Industrial Co., Ltd). The slices were thinner than the original silk fibers. For synchrotron ATR FT-IR, an aluminum disk was used to support the thin silk sections when they were brought into contact with a $100\text{ }\mu\text{m}$ diameter facet tip of the Ge ATR hemisphere (refractive index $n = 4$).

Synchrotron ATR-FTIR mapping measurement was performed using a in-house developed ATR-FTIR device at the IR Microspectroscopy Beamline, which has a high-speed, high-resolution surface characterisation capabilities with spatial resolution down to $1.9\text{ }\mu\text{m}$ [21]. A $100\text{ }\mu\text{m}$ tip ATR accessory for a FT-IR spectrometer (Hyperion 3000, Bruker) with Ge contact lens of $NA = n \sin \varphi \simeq 2.4$ of refractive index $n = 4$ and $\varphi = 36.9^\circ$ a half-angle of the focusing cone was used. A deep sub-wavelength resolution $r = 0.61\lambda_{IR}/NA \simeq 1.5\text{ }\mu\text{m}$ is achievable for the IR wavelengths of interest at the Amide band of $\lambda_{IR} = 1600 - 1700\text{ cm}^{-1}$ or $6.25 - 5.9\text{ }\mu\text{m}$. The nano-IR experiments, i.e., an AFM readout of the height changes in response to IR sample excitation, were carried out with nano-IR2 (Anasys Instruments, Santa Barbara, CA) tool with a $\sim 20\text{ nm}$ diameter

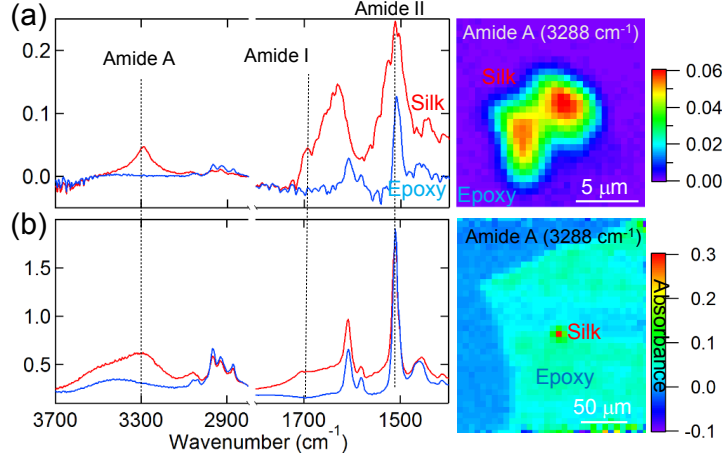


Figure 3. Point spectra and chemical maps of T cross sections of silk (red) in epoxy (blue). (a) Synchrotron ATR-FTIR spectra and its chemical map based on Amide A band. (b) Table-top FT-IR spectra and the corresponding Amide A chemical map. Note that the CCD array has the pixel size of $6.25 \times 6.25 \mu\text{m}^2$ comparable with the T-cross-section of the silk fiber. Chemical maps (on the right-side) are presented as measured (without smoothing).

tip. During continuous scan over the selected region with 0.1 Hz frequency, digitisation was carried out resulting in $25 \times 100 \text{ nm}^2$ pixels in $x \times y$. The oscillation frequency of the AFM needle was 190 kHz. Table-top FT-IR spectrometer (Spotlight, PerkinElmer) was used with a detector array with $\sim 6 \mu\text{m}$ pixel resolution.

Localized modification of silk was carried out via exposure to 515 nm wavelength and 230 fs duration pulses (Pharos, Light Conversion Ltd.) in an integrated industrial laser fabrication setup (Workshop of Photonics, Ltd.). Fibers were imaged and laser radiation was focused using an objective lens of numerical aperture $NA = 0.5$ (Mitutoyo). Single pulse exposures were carried out with pulse energy, E_p . Optical and electron scanning microscopy (SEM) were used for structural characterisation of the laser modified regions.

3. Results and Discussion

A highly crystalline natural silk fiber can be thermally amorphised only through rapid $2 \times 10^3 \text{ K/s}$ thermal quenching from melt [22] as demonstrated for a very tiny amounts of silk measured in nanograms (1 ng occupies a sphere of $5.7 \mu\text{m}$ diameter). Amorphous silk is water soluble and can be used as 3D printing material for scaffolds, desorbable implants [23–25], bio-resists [26], and even be utilised as an electron beam resist [27,28]. Amorphous-to-crystalline transition of silk fibroin is usually achieved via a simple water and alcohol bath processing at moderately elevated temperatures $\sim 80^\circ$ [28]. An UV 266 nm wavelength nanosecond pulsed laser irradiation was also used to enrich amorphous silk fibroin with crystalline β -sheets [29].

To realise a fast thermal quenching and to retrieve the amorphous silk phase [19], we used ultrashort 230 fs duration and 515 nm wavelength laser pulses tightly focused into focal spot of $d = 1.22\lambda/NA \simeq 1.3 \mu\text{m}$; the numerical aperture of the objective lens was $NA = 0.5$ and the wavelength was $\lambda = 515 \text{ nm}$. Single pulse irradiation was carried out to ablate nanograms of silk and create a molten phase which is thermally quenched fast enough [22] to prevent crystallisation (Fig. 1(b)). Threshold of optically recognisable modification of silk fiber during laser irradiation was at 8 nJ which corresponds to 2.8 TW/cm^2 average power (0.6 J/cm^2 fluence) per pulse and is typical for polymer glasses [30].

Nano-IR spectrum, the low-frequency band of the AFM detected height changes in response to a spectral sweep of excitation at the IR absorbance bands at 1 kHz frequency was measured on a transverse (T) microtome cross section of silk fiber embedded into a micro-thin epoxy (Fig. 2(a)). Single wavelength chemical map measured at the specific Amide I band of 1660 cm^{-1} associated with the amorphous silk components is shown in (b) with clearly discernable amorphous rim of the ablation crater, which, in contrast, is not recognisable at the crystalline β -sheet region of 1700 cm^{-1} (inset of (b)). Typical single point measurement spectra are shown in Fig. 2(c) for the Amide I region with clear distinction between epoxy matrix, amorphous, and crystalline counterparts of silk. Amorphous silk of the molten quenched phase has only 200 nm thickness as observed by SEM and AFM, however, it was distinguished using illumination at the corresponding absorption bands ($\lambda_{ex} \simeq 6 \mu\text{m}$).

Thin microtomed slices placed on a high thermal conductivity substrate have been shown to enhance speed of nano-IR imaging since a thermalisation time scale is $t_{th} \simeq \rho c_p h^2 / \eta$ [31], where h is the thickness of the film, η is thermal conductivity, ρ is the mass density, and c_p is the specific heat capacity.

4. Conclusions and outlook

It was shown that by using micro-thin slices which are sub-wavelength at the IR spectral range of interest, it was possible to obtain spectral band readout using nano-IR method - the surface height changes due to thermal expansion following the absorbance spectrum of silk. Amorphous silk created by ultra-fast thermal quenching at the irradiation location of fs-laser pulse was distinguished on the chemical map and imaged with lateral resolution defined by digitisation $x \times y \equiv 25 \times 100 \text{ nm}^2$ and can potentially reach the limit defined by tip [32] which was $20 \times 20 \text{ nm}^2$ in this study. Chemical mapping result acquired using the nano-IR method is consistent with far-field spectroscopy of silk carried out with table-top and synchrotron FT-IR (see Fig. 3(b)). The far-field FT-IR detectors have a typical pixel size of $\sim 6 \mu\text{m}$ which limits the resolution to the entire T-cross-section of the silk fiber, however, a good correspondence with nanoscale IR spectral mapping is confirmed between different spectroscopic methods. Laser-induced amorphisation of crystalline silk has been spectroscopically resolved with high spatial resolution.

We can envisage, that a simple principle of the nano-IR technique allows for a coupling with synchrotron light sources and to complement it with a phase and amplitude mapping using scanning near-field microscopy. The high brightness of synchrotron radiation would also enable a fast mapping required for temporally resolved evolution of photo or thermally excited processes, and even a molecular alignment mapping could be realised by using the four polarisation method [33]. These functionalities will bring new developments into a cutting edge nanoscale molecular characterisation.

Acknowledgments

J.M. acknowledges a partial support by a JSPS KAKENHI Grant No.16K06768. We acknowledge the Swinburne’s startup grant for Nanotechnology facility and partial support via ARC Discovery DP130101205 and DP170100131 grants. Experiments were carried out via beamtime project No. 11119 at the Australian Synchrotron IRM Beamline. Window-on-Photonics R&D, Ltd. is acknowledged for joint development grant and laser fabrication facility.

- [1] Dazzi A, Prater C B, Hu Q, Chase D B, Rabolt J F and Marcott C 2012 *Appl. Spectrosc.* **66** 1365 –1384
- [2] Hillenbrand R, Taubner T and Keilmann F 2002 *Nature* **418** 159 – 162
- [3] Kuznetsov A I, Miroshnichenko A E, Brongersma M L, Kivshar Y S and Lukyanchuk B 2016 *Science* **354** aag2472
- [4] Kruk S, Hopkins B, Kravchenko I I, Miroshnichenko A, Neshev D N and Kivshar Y S 2016 *APL Photonics* **1** 030801
- [5] Woessner A, Alonso-Gonzalez P, Lundeborg M B, Gao Y, Barrios-Vargas J E, Navickaitė G, Ma Q, Janner D, Watanabe K, Cummings A W, Taniguchi T, Pruneri V, Roche S, Jarillo-Herrero P, Hone J, Hillenbrand R and Koppens F H 2016 *Nat. Commun.* **7** 10783
- [6] Ni G X, Wang L, Goldflam M D, Wagner M, Fei Z, McLeod A S, Liu M K, Keilmann F, Özyilmaz B, Neto A H C, Hone J, Fogler M M and Basov D N 2016 *Nat. Photon.* **10** 244 – 248
- [7] Huber M A, Plank M, Eisele M, Marvel R E, Sandner F, Korn T, Schüller C, Haglund R F, Huber R and Cocker T L 2016 *Nano Lett.* **16** 1421 – 1427
- [8] Zenin V A, Andryieuski A, Malureanu R, Radko I P, Volkov V S, Gramotnev D K, Lavrinenko A V and Bozhevolnyi S I 2015 *Nano Lett.* **15** 8271 – 8276
- [9] Khanikaev A B, Arju N, Fan Z, Purtseladze D, Lu F, Lee J, Sarriugarte P, Schnell M, Hillenbrand R, Belkin M A and Shvets G 2016 *Nat. Commun.* **7** 12045
- [10] Fei Z, am M D G, Wu J S, Dai S, Wagner M, McLeod A S, Liu M K, Post K W, Zhu S, Janssen G C A M, Fogler M M and Basov D N 2015 *Nano Lett.* **15** 8271 – 8276
- [11] Yoshioka K, Katayama I, Minami Y, Kitajima M, Yoshida S, Shigekawa H and Takeda J 2016 *Nat. Photon.* **10** 762–765
- [12] Guo J, Bian K, Lin Z and Jiang Y 2016 *J. Chem. Phys.* **145** 160901
- [13] Dazzi A, Prazeres R, Glotin F and Ortega J M 2005 *Opt. Lett.* **30** 2388 – 2390
- [14] Dazzi A, Glotin F and Carminati R 2010 *J. Appl. Phys.* **107** 124519
- [15] Cho S Y, Yun Y S, Lee S, Jang D, Park K Y, Kim J K, amd K Kang B H K, Kaplan D L and Jin H J 2015 *Nat. Commun.* **6** 7145
- [16] Yoshioka T, Tashiro K and Ohta N 2016 *Biomacromolecules* **17** 1437 – 1448
- [17] Hu X, Kaplan D and Cebe P 2006 *Macromolecules* **39** 6161 – 6170
- [18] Yazawa K, Ishida K, Masunaga H, Hikima T and Numata K 2016 *Biomacromolecules* **17** 1057–1066

- [19] Ryu M, Bačytis A, Wang X, Vongsvivut J, Hikima Y, Li J, Tobin M J, Juodkazis S and Morikawa J 2017 *Sci. Reports* **7** 7419
- [20] Maximova K, Wang X W, Balčytis A, Fan L, Li J and Juodkazis S 2016 *Biomicrofluidics* **10** 054101
- [21] Vongsvivut J, Heraud P, Zhang W, Kralovec J A, McNaughton D and Barrow C J 2014 *Food Bioprocess. Technol.* **7** 265A – 277
- [22] Cebe P, Hu X, Kaplan D L, Zhuravlev E, Wurm A, Arbeiter D and Schick C 2013 *Sci. Rep.* **3** 1130
- [23] Li C, Hotz B, Ling S, Guo J, Haas D S, Marelli B, Omenetto F, Lin S J and Kaplan D L 2016 *Biomaterials* **110** 24 – 33
- [24] Li G, Li Y, Cher G, He J, Han Y, Wang X and Kaplan D L 2015 *Adv. Healthc. Mater.* **4** 1134 – 1151
- [25] Tao H, Kaplan D L and Omenetto F G 2012 *Adv. Mater.* **24** 2824 – 2837
- [26] Sun Y L, Li Q, Sun S M, Huang J C, Zheng B Y, Chen Q D, Shao Z Z and Sun H B 2015 *Nat. Commun.* **6** 8612
- [27] Kim S, Marelli B, Brenckle M A, Mitropoulos A N, Gil E S, Tsioris K, Tao H, Kaplan D L and Omenetto F G 2014 *Nat. Nanotechn.* **9** 306 – 310
- [28] Morikawa J, Ryu M, Balčytis A, Seniutinas G, Fan L, Mizeikis V, Li J L, Wang X W, Zamengo M, Wang X and Juodkazis S 2015 *RSC Adv.* **6** 11863 – 11869
- [29] Tsuboi Y, Ikejiri T, Shiga S, Yamada K and Itaya A 2001 *Appl. Phys. A* **73** 637 – 640
- [30] Malinauskas M, Žukauskas A, Hasegawa S, Hayasaki Y, Mizeikis V, Buividas R and Juodkazis S 2016 *Light: Sci. Appl.* **5** e16133
- [31] Katzenmeyer A M, Aksyuk V and Centrone A 2013 *Anal. Chem.* **85** 1972 – 1979
- [32] Wang L, Wang H, Wagner M, Yan Y, Jakob D S and Xu X G 2017 *Science Advances* **3** e1700255
- [33] Hikima Y, Morikawa J and Hashimoto T 2011 *Macromolecules* **44** 3950 – 3957